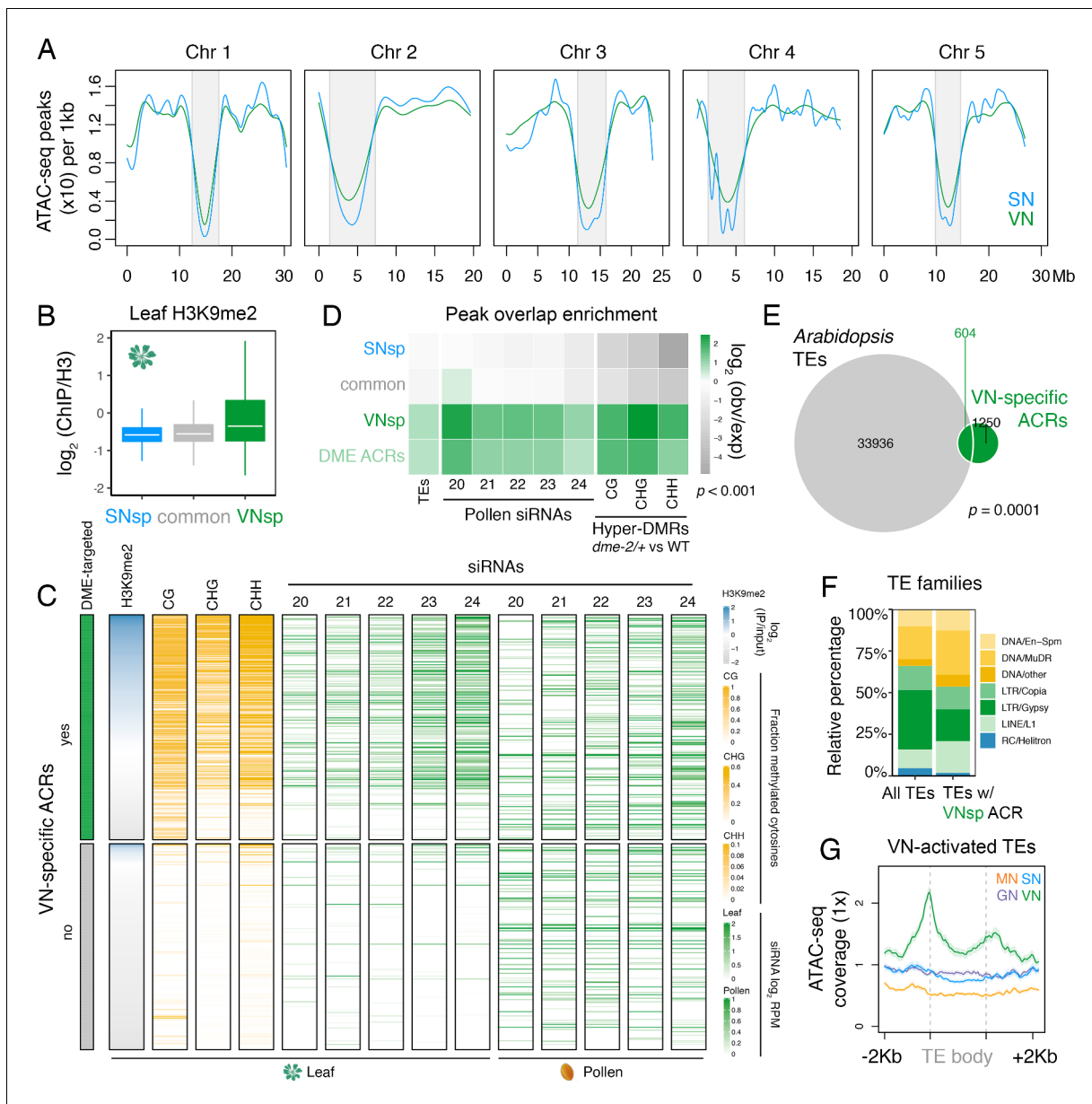


---

## Figures and figure supplements

Epigenetic reprogramming rewires transcription during the alternation of generations in Arabidopsis

**Michael Borg et al**



**Figure 2.** Pericentromeric sequences gain chromatin accessibility in the VN. **(A)** Distribution of accessible chromatin region (ACR) density over the five Arabidopsis chromosomes calculated in 10 kb bins. Pericentromeric regions are indicated with grey shading. **(B)** Levels of H3K9me2 marks in leaf tissue ( $\log_2$  ChIP-seq enrichment relative to H3) (Baerenfaller et al., 2016) at SN-specific, VN-specific, and common ACRs. Each boxplot indicates minimum and maximum values as well as 25th, 50th, and 75th quartiles. **(C)** Heatmap summarising the epigenetic state of VN-specific ACRs. Shown are the  $\log_2$  enrichment of H3K9me2 (relative to H3), the proportion of CG, CHH, and CHG methylation (Stroud et al., 2013) and different size classes of short-interfering RNA (siRNAs) in leaves (Papareddy et al., 2020) alongside pollen siRNAs (Borges et al., 2018). VN-specific ACRs are grouped by the presence or absence of cytosines demethylated by DEMETER (DME) in the VN. **(D)** Heatmap summarising the overlap enrichment of SN-specific, VN-specific, DME-targeted, and common ACRs with TEs, pollen siRNAs (Slotkin et al., 2009), and *dme-2/+* hyper-DMRs. Fold changes were determined using hypergeometric tests compared with random Arabidopsis genomic regions ( $n = 10,000,000$  permutations). **(E)** Pairwise overlap between VN-specific ACRs and Arabidopsis transposable elements (TEs). Significance of the enriched overlap ( $p$ -value) was determined in the hypergeometric test shown in panel C. **(F)** Distribution of TE gene classes associated with VN-specific ACRs alongside the relative frequency in the Arabidopsis genome. **(G)** Averaged ATAC-seq enrichment over TE genes specifically re-activated in the VN. Plotted is the ATAC-seq signal normalised to 1× Arabidopsis genome coverage.

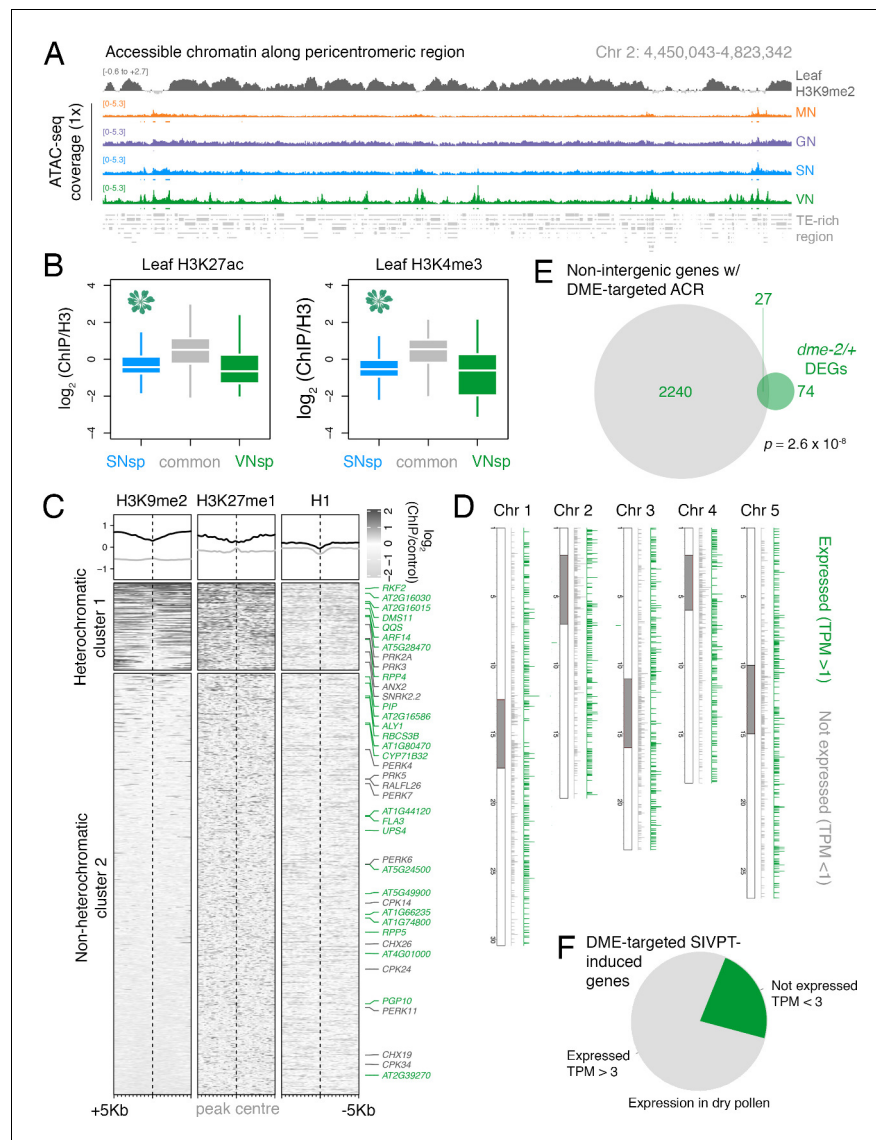


**Figure 2—figure supplement 1.** DEMETER (DME) demethylates accessible chromatin uniformly across the VN. (A) Genome browser view of the ATAC-seq data sets over a TE-rich pericentromeric region of chromosome 2. Tracks represent the levels of H3K9me2 in leaf ( $\log_2$  ChIP-seq enrichment relative H3) and the ATAC-seq signal normalised to 1 $\times$  Arabidopsis genome coverage for nuclei of microspores (MN), germ cells (GN), sperm (SN), and vegetative cells (VN). (B) Levels of active H3K27ac and H3K4me3 marks in leaf tissue ( $\log_2$  ChIP-seq enrichment relative H3) at SN-specific, VN-specific, and common accessible chromatin regions (ACRs). Each boxplot indicates minimum and maximum values as well as 25th, 50th, and 75th quartiles. (C) Levels of constitutive heterochromatin marks in leaf tissue centred over non-intergenic DME-targeted ACRs. Clustering is based on H3K9me2 levels. Plotted is the  $\log_2$  ChIP-seq enrichment relative H3 (H3K9me1 and H3K27me1) or input (H1). Numbers of ACRs are  $n = 407$  (cluster 1) and  $n = 1,966,966$  (cluster 2). Genes mis-expressed in *dme-2/+* mutant pollen compared to wild type (WT; green) and genes induced during pollen tube growth (grey) are marked. (D) Distribution of DME-targeted ACRs across all five chromosomes of the Arabidopsis genome. Expressed genes (TPM > 1) associated with a DME-targeted ACR are shown in green while non-expressed genes (TPM < 1) are shown in grey. Pericentromeric regions are indicated with grey shading. (E) Differentially expressed genes (DEGs) in *dme-2/+* compared to WT ( $n = 101$ ) and genes associated with non-intergenic DME-targeted ACRs ( $n = 2267$ ) significantly overlap each other. Significance of the enriched overlap ( $p$ -value) was determined using a two-sided Fisher's exact test. (F) Dry pollen expression of DME-targeted genes induced during semi in vivo pollen tube growth (Leydon et al., 2017).

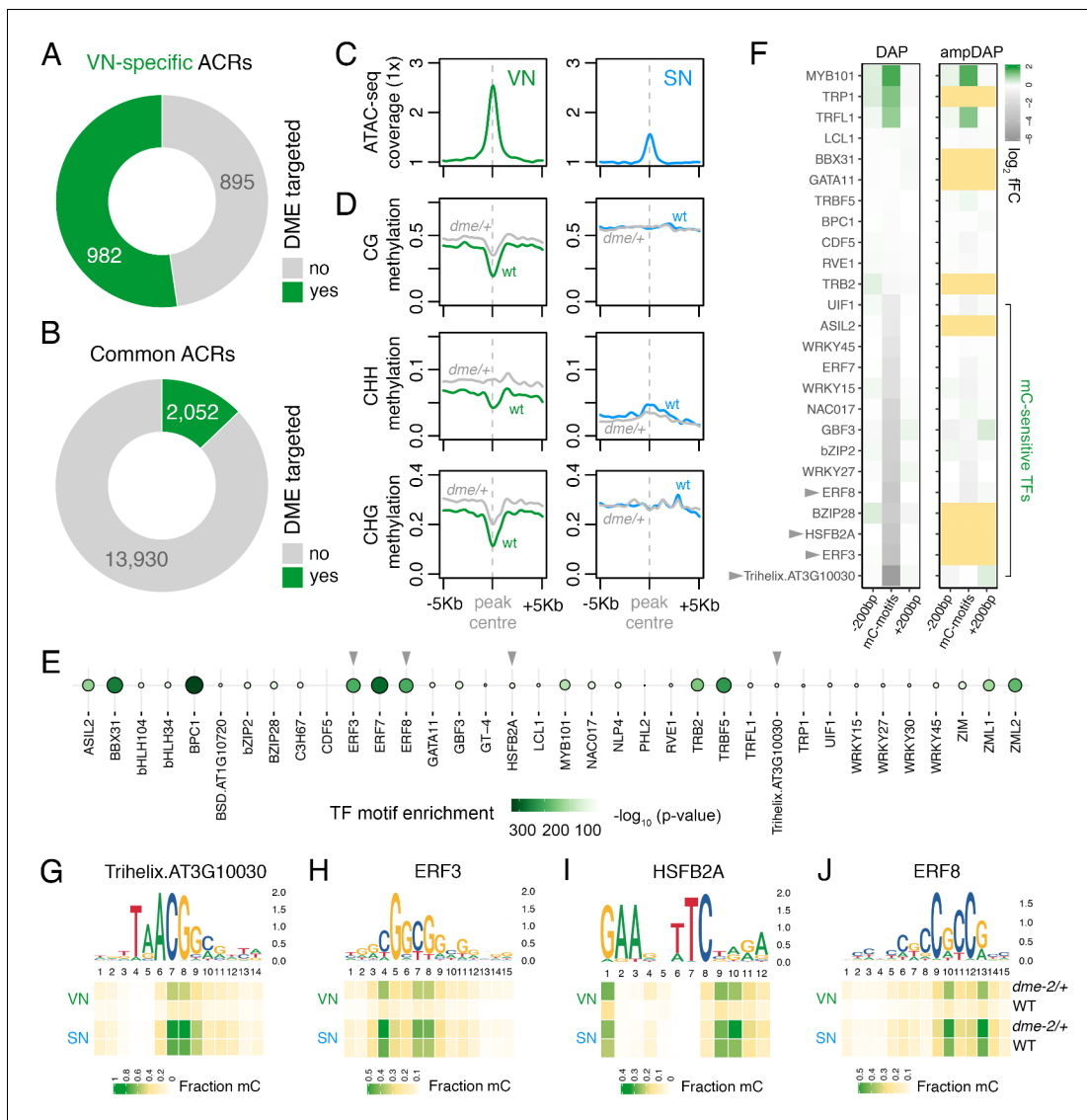


**Figure 3.** DEMETER (DME) demethylates predicted TF binding sites in accessible chromatin. (A and B) Relative proportion of VN-specific accessible chromatin regions (ACRs) (A) and common ACRs (B) that overlap with cytosines demethylated by DME in the VN. (C and D) Averaged metaplots comparing ATAC-seq enrichment (C) and the proportion of CG, CHH, and CHG methylation (D) in sperm (blue) and the VN (green) over DME-targeted ACRs. Regions with at least five differentially methylated cytosines were plotted. Coloured lines represent wild-type (WT) levels while grey lines indicate the level in nuclei isolated from *dme-2/+* mutant pollen. (E) Motifs of VN-expressed TFs enriched within DME-targeted ACRs. Significance (p-value) was assessed using a two-sided Fisher's exact test. TFs shown in panels F–I are marked with grey triangles. (F) Binding preference for the VN-expressed TF motifs enriched within DME-targeted ACRs. Left: DAP-seq binding fold-change at methylated motifs (mC-motifs) relative to neighbouring motifs ( $\pm 200$  bp). Right: ampDAP-seq binding fold-change at the same mC-motifs without DNA methylation. Yellow boxes indicate TFs without a score due to too few motifs. Data is from previously published DAP-seq experiments (O'Malley et al., 2016). TFs shown in panels F–I are marked with grey triangles. (G–J) DNA methylation level at predicted binding sites within DME-targeted ACRs for the four highest methylation-sensitive TFs shown in panel E – Trihelix.AT3G10030 (G), ERF3 (H), HSFB2A (I), and ERF8 (J). Each heatmap summarises the proportion of methylated cytosines over predicted binding sites in VN and SN of WT and *dme-2/+* pollen. Single nucleotides are indicated by the corresponding position frequency matrix logo plotted above each heatmap.

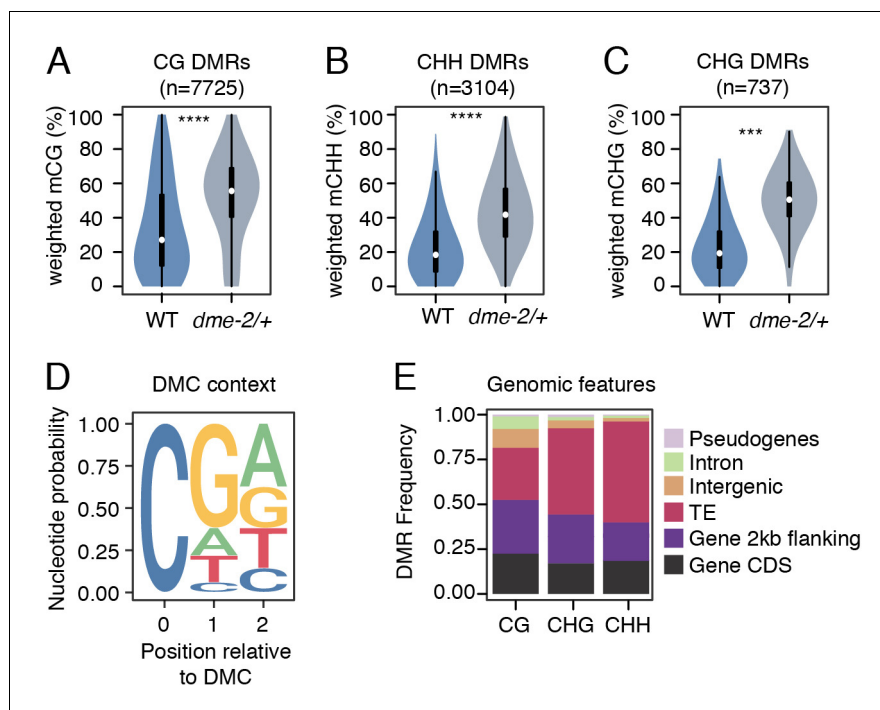


**Figure 3—figure supplement 1.** Differential methylated region (DMR) analysis between VN from wild-type (WT) and *dme-2/+* mutant pollen. (A–C) Violin plots showing weighted DNA methylation rates of DMRs in CG (A), CHH (B), and CHG (C) context. Each overlaid boxplot indicates minimum and maximum values as well as 25th, 50th, and 75th quartiles. p-values  $<2.2 \times 10^{-16}$  and  $<1.6 \times 10^{-4}$  based on Mann–Whitney U-test of methylation differences between WT and *dme-2/+* are represented by \*\*\*\* and \*\*\* respectively. (D) Nucleotide probability of significant differentially methylated cytosines (DMCs) within DMRs in VN from *dme-2/+* pollen compared to WT. (E) Proportion of genomic features overlapping CG, CHG, and CHH DMRs.

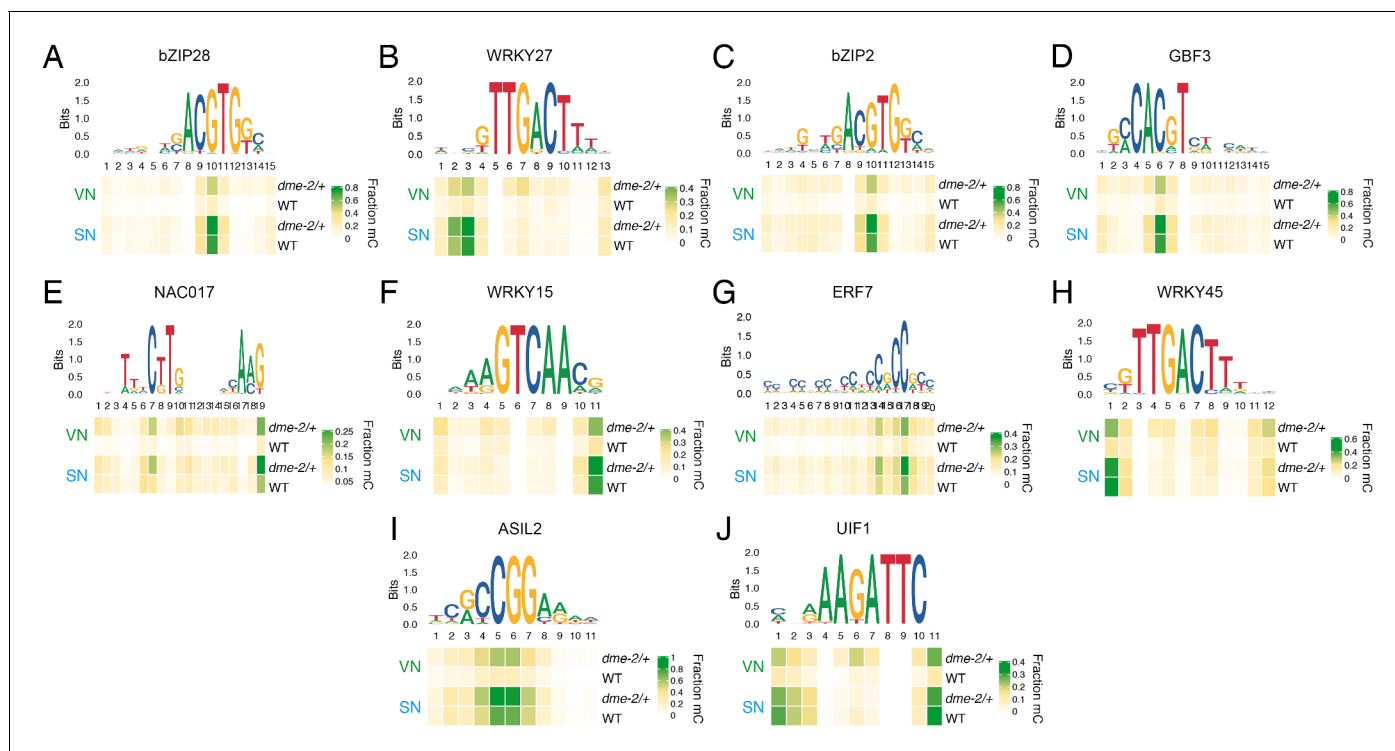


**Figure 3—figure supplement 2.** DEMETER (DME) demethylates predicted TF binding sites specifically in the VN. (A–J) DNA methylation level at predicted binding sites within DME-targeted accessible chromatin regions (ACRs) for the remaining 10 methylation-sensitive TFs shown in **Figure 4E** – bZIP28 (A), WRKY27 (B), bZIP2 (C), GBF3 (D), NAC017 (E), WRKY15 (F), ERF7 (G), WRKY45 (H), ASIL2 (I), and UIF1 (J). Each heatmap summarises the proportion of methylated cytosines over the predicted binding sites in VN and SN of wild-type (WT) and *dme-2/+* pollen. Single base pair positions are indicated by the corresponding position frequency matrix logo plotted above each heatmap.

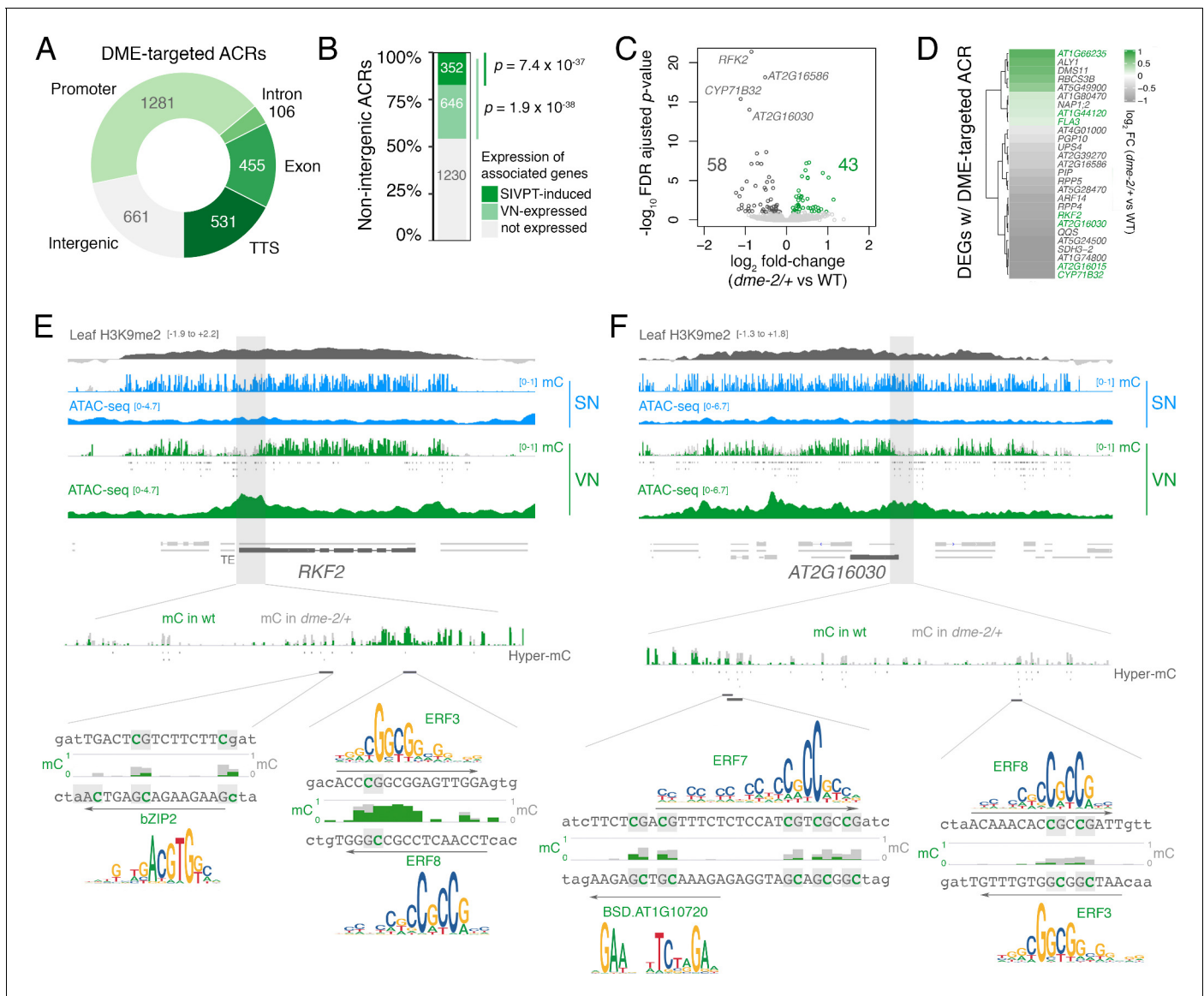


**Figure 4.** DEMETER (DME) activity regulates the expression of pollen tube-related genes. **(A)** Distribution of genomic features associated with DME-targeted accessible chromatin regions (ACRs). **(B)** Expression status of genes lying in the vicinity ( $< 900$  bp) of a DME-targeted ACR. Genes were classified as being expressed in the VN (TPM  $> 1$ , light green) or by being upregulated during semi in vivo pollen tube (SIVPT) growth (dark green) (Leydon et al., 2017). Statistical enrichment of the overlap was determined using pairwise two-sided Fisher's exact tests. **(C)** Volcano plot of differentially expressed genes (DEGs) in *dme-2/+* pollen compared to wild type (WT). Upregulated genes are shown in green while downregulated genes are shown in dark grey. DEGs were defined as having an FDR-adjusted  $p$ -value  $< 0.1$ . The top four most significantly downregulated genes are labelled. **(D)** Heatmap illustrating the magnitude of expression changes for DME-dependent DEGs directly associated with a DME-targeted ACR. Plotted is the  $\log_2$  fold-change in *dme-2/+* pollen compared to WT. VN-specific genes are highlighted in green. **(E and F)** Browser view of two VN-specific direct DME target genes – *RECEPTOR-LIKE SERINE/THREONINE KINASE (RKF2)* (E) and the *AT2G16030* locus encoding a SAM-dependent methyltransferase (F). Both genes are marked with H3K9me2 in the sporophyte ( $\log_2$  ChIP-seq enrichment relative to H3). Tracks illustrate ATAC-seq signals and the proportion of methylated cytosines in all contexts (mC) in SN (blue) and VN (green), with DNA methylation levels in *dme-2/+* overlaid in grey. DME-dependent hyper-methylated cytosines (HMCs) are marked below. Shading indicates the flanking promoter region shown in the close-up view. Sequences surrounding predicted TF binding sites are shown, with the level of cytosine methylation at HMCs highlighted in green and grey for WT and *dme-2/+*, respectively. Arrows indicate the orientation and position of TF motifs with a corresponding position frequency matrix logo plotted above.



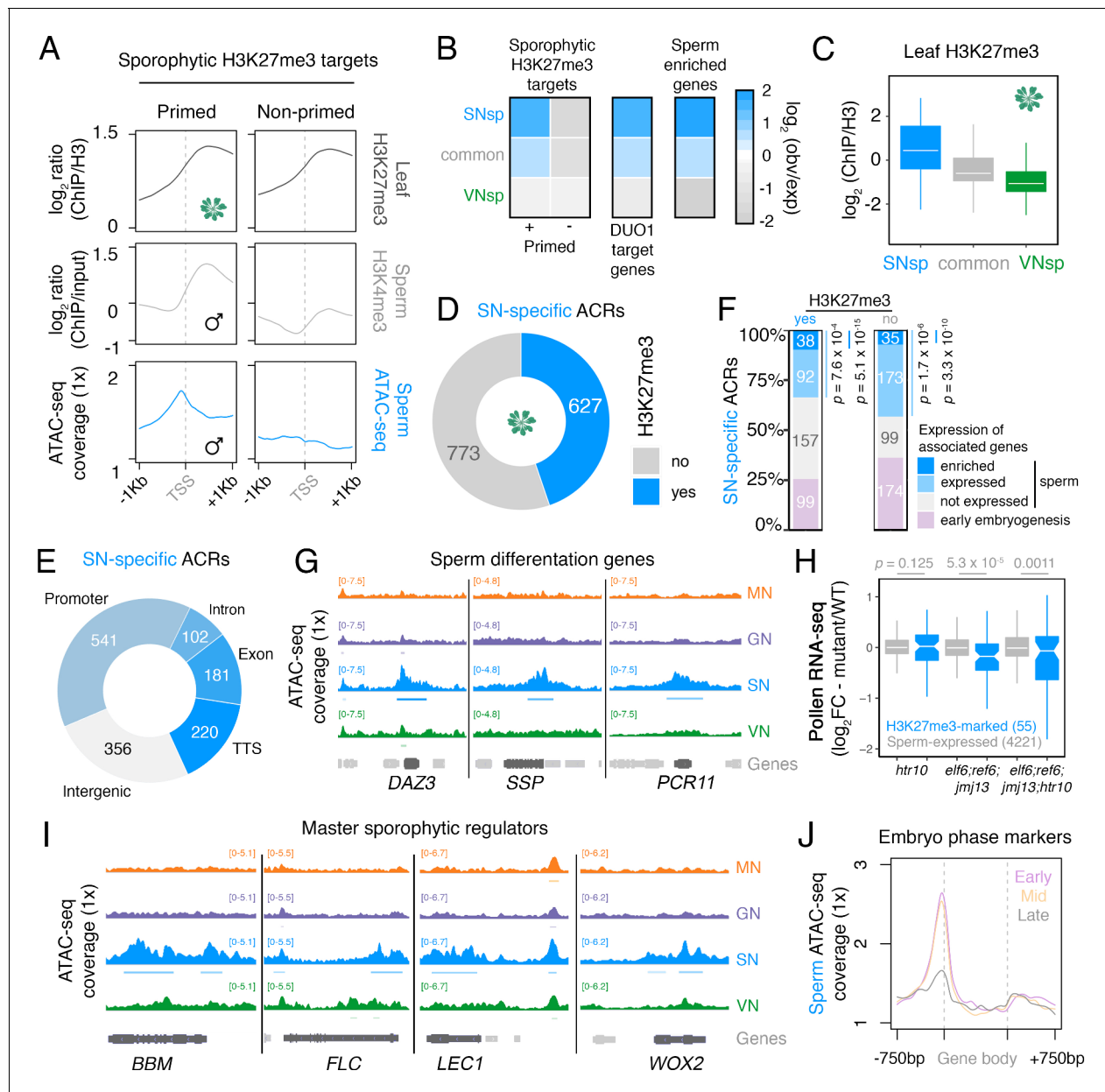


**Figure 5.** Chromatin accessibility in sperm forecasts sporophytic development. (A) Sperm ATAC-seq profiles reflect the reprogrammed state of sporophytic H3K27me3 target genes. Plotted are averaged levels of leaf H3K27me3 and sperm H3K4me3 ( $\log_2$  ChIP-seq enrichment relative to control) together with sperm ATAC-seq signals. ChIP-seq data and clustering for the presence and absence of H3K4me3 enrichment in sperm were described previously (Borg et al., 2020). (B) Heatmap summarising the overlap enrichment of SN-specific, VN-specific, and common accessible chromatin regions (ACRs) with somatic Polycomb target genes, DUO1 target genes, and sperm-enriched genes. Fold-enrichment was determined using hypergeometric tests compared with random Arabidopsis genomic regions ( $n = 10,000,000$  permutations). (C) Levels of H3K27me3 marks in leaf tissue ( $\log_2$  ChIP-seq enrichment relative to H3) at SN-specific, VN-specific, and common ACRs. Each boxplot indicates minimum and maximum values as well as 25th, 50th, and 75th quartiles. (D) Relative proportion of SN-specific ACRs that overlap with a somatic H3K27me3 domain. (E) Distribution of genomic features associated with SN-specific ACRs. (F) Expression status of genes in the vicinity ( $<900$  bp) of an SN-specific ACR with or without H3K27me3 in the sporophyte. Genes were classified as being expressed in sperm (TPM  $>1$ , light blue), by having enriched expression in sperm (dark blue), or by expression in the early zygote or embryos but not sperm (pink). Non-expressed genes in sperm are shown in grey. TPM  $>1$  or  $<1$  was used as a threshold for expressed and non-expressed genes, respectively. Statistical enrichment was determined using pairwise two-sided Fisher's exact tests. (G) Chromatin accessibility at three sperm-specific genes associated with sperm differentiation – *DUO1-ACTIVATED ZINC FINGER 1* (*DAZ1*), *SHORT SUSPENSOR 1* (*SSP1*) and *PLANT CADMIUM RESISTANCE 11* (*PCR11*). Tracks represent the ATAC-seq signal normalised to  $1 \times$  Arabidopsis genome coverage for nuclei of the microspore (MN), germ cell (GN), sperm (SN), and vegetative cell (VN). (H) Differential expression between *htr10*, *elf6;ref6*; *jmj13*, and *elf6;ref6;jmj13;htr10* pollen relative to wild type (WT). Each boxplot indicates the minimum and maximum values as well as 25th, 50th, and 75th quartiles. (I) Master sporophytic regulators. Tracks represent the ATAC-seq signal normalised to  $1 \times$  Arabidopsis genome coverage for nuclei of the microspore (MN), germ cell (GN), sperm (SN), and vegetative cell (VN). (J) Embryo phase markers. Sperm ATAC-seq coverage ( $1 \times$ ) is shown for Early, Mid, and Late embryo phases.



## Figure 5 continued

75th quartiles. Sample size ( $n$ ) of genes associated with an H3K27me3-repressed ACR (blue) and all sperm-expressed genes (grey) is shown. Plot is restricted to genes with >10 counts in at least one RNA-seq sample and/or replicate. Statistical analysis was performed using two-sided Kolmogorov–Smirnov tests. (I) Chromatin accessibility at four major developmental regulators transcribed during early sporophyte development – *BABY BOOM* (*BBM*), *FLOWERING LOCUS C* (*FLC*), *LEAFY COTYLEDON 1* (*LEC1*), and *WUSCHEL-RELATED HOMEBOX 2* (*WOX2*). Tracks represent the ATAC-seq signal normalised to 1× Arabidopsis genome coverage for nuclei of the microspore (MN), germ cell (GN), sperm (SN), and vegetative cell (VN). (J) Averaged ATAC-seq enrichment over genes with enriched expression during early (pink), mid (yellow), and late (grey) embryogenesis, which represent the pre-cotyledon phase, the transition phase, and the mature green phase, respectively (*Hofmann et al., 2019*). Plotted is the sperm ATAC-seq signal normalised to 1× Arabidopsis genome coverage.